Dynamics of Nanodroplets on Vibrating Surfaces

LANGMUIR Article
Cite This: Langmuir 2018, 34, 11898−11904
pubs.acs.org/Langmuir

Dynamics of Nanodroplets on Vibrating Surfaces

Rohit Pillai,* Matthew K. Borg, and Jason M. Reese

School of Engineering, University of Edinburgh, Edinburgh EH9 3FB, United Kingdom

ABSTRACT: We report the results of molecular dynamics investigations into the behavior of nanoscale water droplets on surfaces subjected to cyclic-frequency normal vibration. Our results show, for the first time, a range of vibration-induced phenomena, including the existence of the following different regimes: evaporation, droplet oscillation, and droplet lift-off. We also describe the effect of different surface wettabilities on evaporation. The outcomes of this work can be utilized in the design of future nanoengineered technologies that employ surface/bulk acoustic waves, such as water-based cooling systems for high-heat-generating processor chips, by tuning the vibration frequency and amplitude, as well as the surface wettability, to obtain the desired performance.

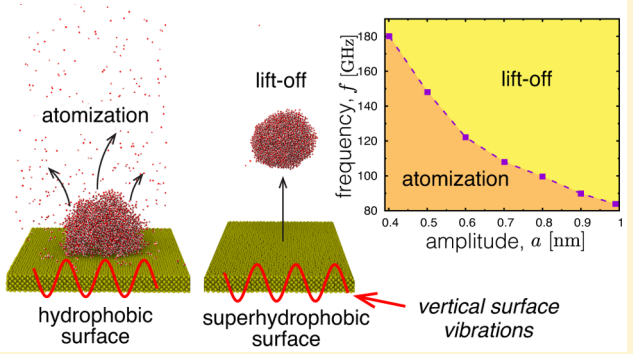

INTRODUCTION

The dynamical behavior of drops and interfaces subjected to free or forced vibrations are classical problems in hydrodynamics, with rich literature dating back to the late 19th century.[1] Early interest was driven by the fundamental science of interfacial instabilities, with the focus on generating analytical expressions for capillary free-surface oscillations and their stability.[2,3] In the mid 20th century, there were significant theoretical developments in understanding "acoustic streaming", or flow fields generated by sound attenuation within a fluid.[4,5]

There has been renewed interest in this area in recent years, with experimental research showing that high-frequency bulk/surface vibrations of the supporting substrate can disintegrate liquids into a fine mist of droplets.[6−8] This has numerous applications in the chemical, medical, and information/communications technology industries.[9−11] For example, precisely controlling micro/nanoscale droplets inside lab-on-a-chip devices using surface acoustic waves (SAW).[12]

Current experiments on droplet atomization using SAW typically employ frequencies in the MHz−GHz range and amplitudes of nanometres.[13] However, in principle, bulk/surface vibrations in the GHz−THz range are realizable,[14−17] which is a hitherto unexplored parameter-space that is the subject of this present paper. Existing numerical studies of the effects of vibration on sessile droplets[18−24] have two drawbacks that make them unsuitable for the problem considered here; first, they are limited to low frequencies, as the time-scale separation (between the rapid acoustics and the slower hydrodynamics) inherent to high-frequency acoustofluidics is challenging to simulate. Second, the droplet interface is typically assumed to be unperturbed throughout the simulation, with the focus on the acoustic streaming within the liquid. No droplet deformation or atomization is considered. In this paper, we address these limitations by using molecular dynamics (MD) to study, for the first time, the behavior of water droplets on vibrating surfaces; there is no other simulation tool that offers the high-fidelity required to resolve these very short spatio-/temporal-scales.

MODELING METHODOLOGY

Molecular Dynamics. Molecular dynamics (MD) simulations solve Newton's equations of motion for each molecule in the domain:

$$\boldsymbol{F}_i = m_i \frac{d\boldsymbol{v}_i}{dt} = \sum_{j\neq i}^{N} -\nabla U_{ij}(r_{ij}) \tag{1}$$

$$\boldsymbol{v}_i = \frac{d\boldsymbol{r}_i}{dt} \tag{2}$$

where $\boldsymbol{F}_i$, $\boldsymbol{v}_i$, and $\boldsymbol{r}_i$ are the force, velocity, and position, respectively, of molecule "i" of mass m_i at time t, N is the total number of molecules, and $U_{ij}(r_{ij})$ is the intermolecular potential between the i^{th} and j^{th} molecule, with r_{ij} the distance between them. In our simulations, all atoms interact using a combined 12−6 Lennard-Jones and Coulomb potential:

$$U_{ij}(r_{ij}) = 4\lambda\epsilon_{ij}\left[\left(\frac{\sigma_{ij}}{r_{ij}}\right)^{12} - \left(\frac{\sigma_{ij}}{r_{ij}}\right)^{6}\right] + \frac{q_i q_j}{4\pi\epsilon_0 r_{ij}} \tag{3}$$

where σ is the distance at which the interatomic potential is zero, ϵ is the depth of the potential well, q is the charge of the atomic site, and ϵ_0 is the vacuum permittivity. The λ parameter in eq 3 allows the solid−liquid interaction strength, and hence the surface wettability, to be modified from superhydrophobic

Received: June 18, 2018
Revised: August 21, 2018
Published: August 21, 2018

DOI: 10.1021/acs.langmuir.8b02066
Langmuir 2018, 34, 11898−11904

($\lambda \approx 0.15$, $\theta \approx 160°$, where θ is the static contact angle of the nanodroplet at equilibrium) to superhydrophilic ($\lambda \approx 1$, $\theta < 20°$). For all liquid−liquid and solid−solid interactions, $\lambda = 1$. The first term on the right side of eq 3 represents the intermolecular forces, while the second term represents the electrostatic contributions. For computational efficiency, we truncate the intermolecular and electrostatic force calculations at radial distances of 1.2 and 1.3 nm, respectively. Long-range electrostatics are incorporated using the particle−particle particle−mesh (PPPM) method, with a relative tolerance of 10^{-6}.

Polar water molecules are modeled using the rigid four-site TIP4P/2005 model;[25] this consists of one oxygen (O) site, two charged hydrogen (H) sites, and one massless charged (M) site located along the bisector of the hydrogen atoms, at a distance of 0.1546 Å from the oxygen atom. The internal geometry of the water molecule is constrained by specifying a fixed O−H bond distance (0.9572 Å) and H−O−H angle (104.52°); this structure is maintained using the SHAKE algorithm.[26] The droplet-supporting substrate consists of seven layers of metal atoms in a FCC lattice, with a lattice constant of 3.92 Å. All the interatomic potential parameters are listed in Table 1. The cross interactions between different atomic sites

Table 1. Interatomic Potential Parameters and Atomic Masses (m_a) for Sites in TIP4P/2005 Water Molecules (H, O, and M), and Substrate (S) Atoms

site	ϵ (kJ/mol)	σ (Å)	q (e)	m_a (u)
H	0	0	0.5242	1.00800
O	0.774	3.1589	0	15.9994
M	0	0	−1.0484	0
S	4.18	2.471	0	195.084

are specified by the Lorentz−Berthelot mixing rules, $\epsilon_{ij} = \sqrt{\epsilon_i \epsilon_j}$ and $\sigma_{ij} = (\sigma_i + \sigma_j)/2$. Time integration of all molecule trajectories is achieved using the velocity-Verlet algorithm, with a time step of 2 fs. We performed all the simulations using the open-source MD software LAMMPS.[27]

Simulation Setup. The initial setup, as shown in Figure 1, consists of a droplet of water molecules initialized on an atomically smooth substrate (S). The domain boundaries are set to be periodic in every direction, and a superhydrophilic barrier is positioned far above the substrate to collect atomized molecules and prevent them from leaving the domain via the top boundary and re-entering through the bottom boundary (see Figure 1). This barrier consists of a layer of metal atoms identical to the substrate, but with a large artificial solid−liquid interaction strength ($\lambda = 5$) to make it extremely hydrophilic. The values of σ, ϵ, and atomic mass m for the substrate/barrier atoms are derived from those of platinum, to represent a metal substrate typical of nanoacoustic applications.

The MD simulation setup in Figure 1 comprises a water droplet of N_0 water molecules placed on a substrate and equilibrated for 1 ns at a constant temperature of 300 K. Following equilibration, the simulation is run for a production time of 1−2 ns, during which the substrate is oscillated vertically at gigahertz-order frequencies, for a range of amplitudes a, frequencies f, and substrate wettabilities λ. Temperature control is not applied to the water molecules during the production time, but the substrate and barrier molecules are coupled to a Berendsen thermostat to maintain the surface at 300 K. Three sets of simulations are carried out

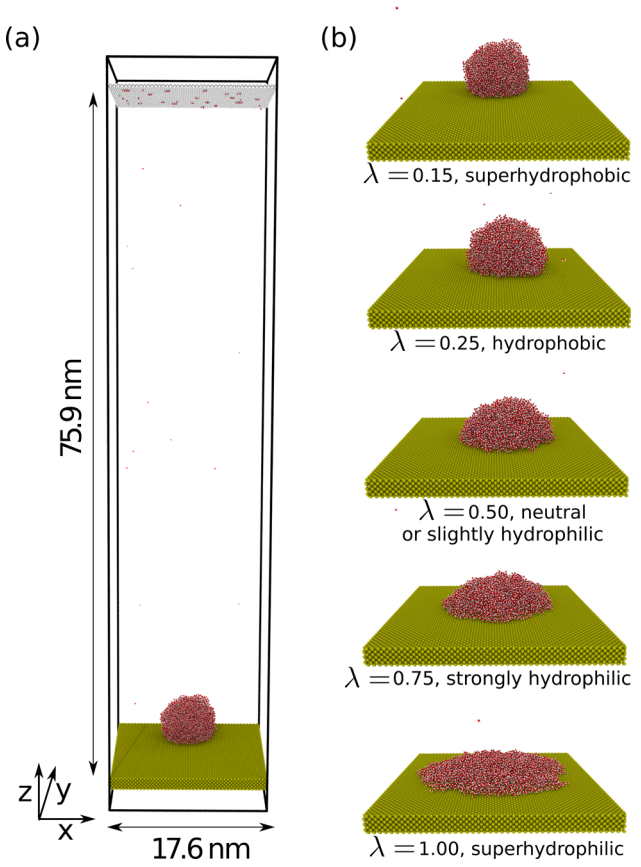

Figure 1. (a) Schematic of the MD domain, with the substrate at the bottom, and (b) initial snapshots of droplets equilibrated on surfaces of different wettabilities; from top to bottom: $\lambda = 0.15$ (superhydrophobic, $\theta \approx 160°$), 0.25 (hydrophobic, $\theta \approx 100°$), 0.50 (neutral or slightly hydrophilic, $\theta \approx 40°$), 0.75 (strongly hydrophilic, $\theta \approx 20°$), and 1.00 (superhydrophilic, $\theta < 20°$).

for droplets containing 2000 ($R \approx 3$ nm), 3000 ($R \approx 3.5$ nm), and 4500 ($R \approx 4$ nm) molecules, respectively. The specified radii R are calculated assuming a hemispherical shape for each droplet.

One of the key measurements in these simulations relies on tracking how many molecules are "atomized". We classify a water molecule as atomized if:

(1) Its number of neighboring water molecules is fewer than 10 (where two water molecules are considered neighbors if $r_{ij} < 6.3$ Å), or
(2) Its vertical distance from the top of the substrate is greater than 10 nm.

The first criterion is used to identify vapor molecules,[28,29] while the second accounts for the atomization of liquid molecules en masse; N_A then represents the total number of atomized molecules at every time-step.

Once the atomized molecules are identified, the temperature T_f of the remaining droplet (comprising nonatomized water molecules) can be calculated using the equipartition theorem:

$$T_f = \frac{1}{N_f} \sum_{i=1}^{N_f} \frac{2}{3k_B} \sum_{n=1}^{3} \frac{1}{2} m_i (v_{i,n} - \overline{v}_n)^2 \quad (4)$$

where $N_f = N_0 - N_A$ is the number of water molecules remaining in the droplet, k_B is the Boltzmann constant, $v_{i,n}$ is the velocity of molecule i in the n (= x, y, z) direction, and $\overline{v}_n$ is

DOI: 10.1021/acs.langmuir.8b02066
Langmuir 2018, 34, 11898−11904

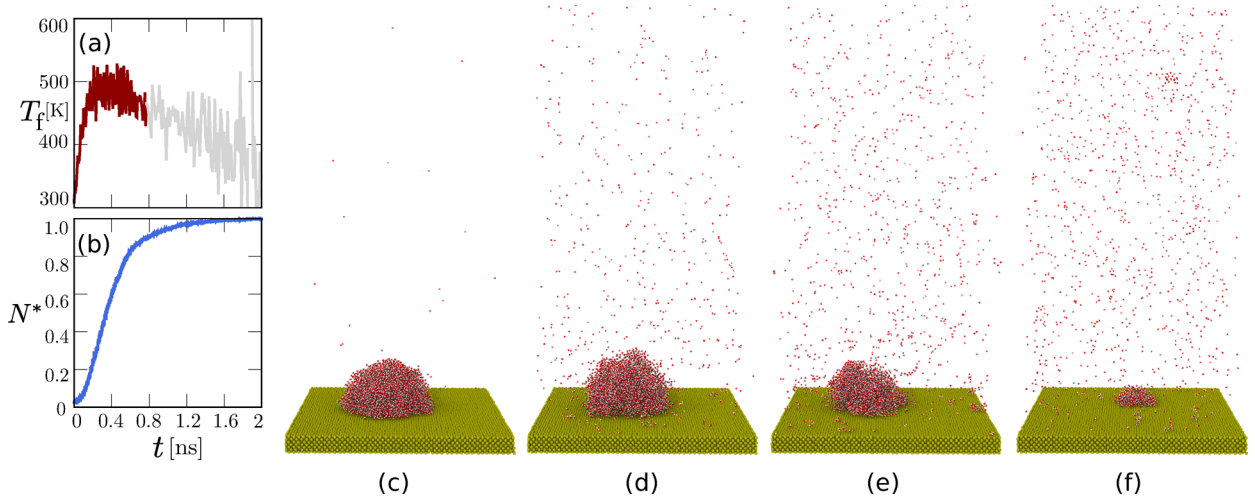

Figure 2. Temporal evolution of (a) the temperature inside the water droplet, and (b) the atomization of the water molecules. Snapshots (c–f) show the effect of vibration-induced evaporation at times t = 0.25, 0.50, 0.75, and 1.00 ns, respectively. Case parameters: N_0 = 4500, λ = 0.5, a = 0.375 nm, and f = 100 GHz. The use of light gray indicates that our error threshold in the temperature measurements is exceeded.

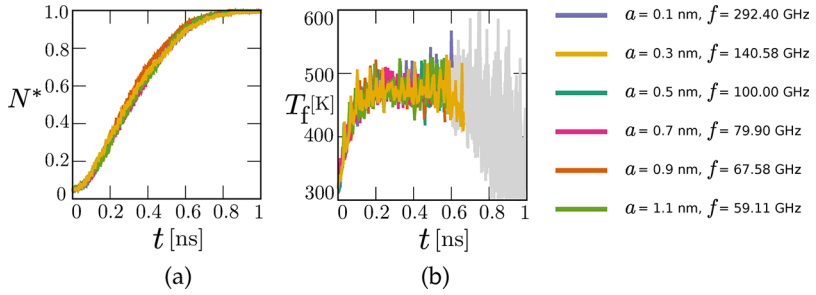

Figure 3. Temporal evolution of (a) atomization, and (b) temperature for multiple combinations of a and f that give a fixed A^*; N_0 = 3000 and λ = 0.5 in all cases. The use of light gray indicates that our error threshold in the temperature measurements is exceeded.

the mean flow velocity in the n direction due to the induced oscillations. To prevent erroneous temperature values, care must be taken both to exclude the atomized molecules and to subtract the droplet center-of-mass velocity from each water molecule, prior to calculating the temperature.

RESULTS AND DISCUSSION

Nanodroplet Evaporation. Our MD simulations show that when nanoscale droplets or films are exposed to substrate vibrations, atomization occurs primarily due to heating; acoustothermal heating and evaporation has been observed experimentally for microscale droplets and thin films,[30−32] but here we report it for nanodroplets for the first time. The temperature within the droplet (calculated using eq 4), and the scaled atomization rate N^* (= N_A/N_0) give an indication of this heating effect. Figure 2(a,b) show these two measurements for a typical case of a droplet evaporating on an oscillating surface (with the vibration and wettability characteristics as specified in the figure caption), while Figure 2(c,f) show temporal snapshots from the MD simulation. In this case, significant heating is observed inside the droplet, with temperatures peaking at 500 K before dropping off to 450 K.

Note that large temperature fluctuations (also known as "thermal noise") are observed in Figure 2(a) when t > 0.8 ns. This is because of the very small number of molecules remaining in the droplet. The fractional error in temperature measurements (E_T) can be calculated as $E_T = \sqrt{k_B/MN_f c_v}$,[33] where c_v is the per-molecule specific heat capacity at constant volume. The thermal noise can only be improved in these tiny residual droplets if many more (i.e., M) statistically independent simulations are run and averaged; we instead do not draw any conclusions from our temperature measurements whenever the fractional error E_T exceeds 0.5 (i.e., a relative error of 50%). This is indicated in Figure 2, and following figures, by the use of light gray lines replacing the original line color when the specified threshold in E_T is exceeded.

From the MD snapshots, the evaporation process appears to be uniform, and the droplet shrinks evenly without any change in the center-of-mass position relative to the x, z coordinate axes (see Figure 2(c–e)). Movement on the substrate is only observed once the droplet has lost most of its molecules (Figure 2(f)).

We can characterize the acoustothermal evaporation of these nanoscale droplets by the ratio of the force applied by the vibrating substrate, given by $F_{vib} \approx m_f a(2\pi f)^2$, to the resulting viscous dissipation of the applied vibrations, as defined by the internal energy gained by the water molecules, given by $F_{vis} \approx m_f \mu v_{ref}^2 t_a / L_{ref}^3$. Here, m_f, μ, t_a, v_{ref}, and L_{ref} are the mass of the droplet, fluid viscosity, acoustic time scale (t_a= 1/f), reference velocity scale ($v_{ref} = \sqrt{k_B T_0/m_i}$), and reference length scale ($L_{ref} = \sqrt{\mu/2\rho\pi f}$), respectively. This ratio of competing vibration/dissipation forces produces a nondimensional *acoustothermal atomization parameter*:[34]

DOI: 10.1021/acs.langmuir.8b02066
Langmuir 2018, 34, 11898−11904

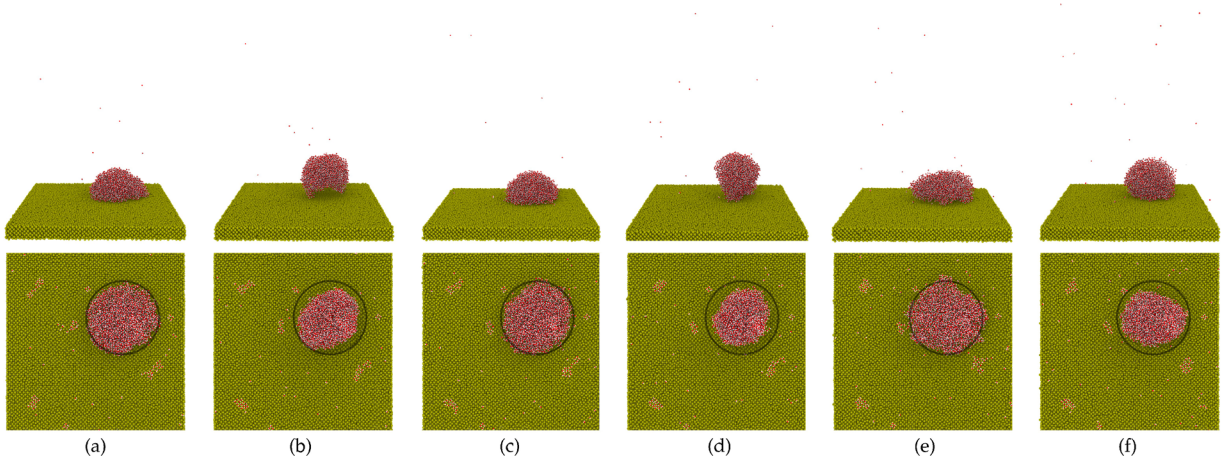

Figure 4. Snapshots of side and top views of nanodroplet vibration for a = 1.1 nm and f = 59.11 GHz, at times t = 0, 0.01, 0.02, 0.03, 0.04, and 0.05 ns, with N_0 = 3000 and λ = 0.5. A black circle corresponding to the initial droplet dimensions has been superimposed on all the top view snapshots; this is to help show the variations in droplet shape during the oscillations.

$$A^* = \frac{F_{vib}}{F_{vis}} = K\sqrt{\frac{2\pi\mu}{\rho^3}}\frac{m_i}{k_B T_0} a f^{3/2} \quad (5)$$

which has a nondimensional scaling prefactor K. Physically, increasing A^* can be interpreted as increasing the energy added to the fluid by the vibrating substrate. If this scaling is appropriate, then the evaporation dynamics for a fixed A^* should be independent of the values of the vibration parameters a and f.

To test the validity of this scaling for acoustothermal droplet evaporation, multiple cases with a fixed A^* were simulated, but with different combinations of a and f. The temporal evolutions of the atomization and droplet temperature are plotted in Figure 3. Despite the large variation in acoustic parameters (for example, f is varied from ∼60−292 GHz), the evaporation rate (Figure 3(a)) and temperature profiles (Figure 3(b)) are identical for all cases, therefore validating our proposed scaling relationship for evaporating nanodroplets.

Nanodroplet Oscillation: Approaching Lift-Off. It has recently been shown in macroscale experiments[35] that the apparent wettability of a surface increases linearly with vibration amplitude a, but is independent of the vibration frequency f. Similarly, the magnitude of the (acoustic) pressure field within a macroscale drop increases during unidirectional motion of the substrate, and depends on the amplitude of vibration. The increase in acoustic pressure is higher at larger amplitudes and lower frequencies, but the acoustic pressure does not build for higher frequencies.[31]

The impact of acoustic pressure on nanodroplet vibration can be evinced by comparing the extremal cases from Figure 3, namely those corresponding to a = 0.1 nm (small amplitude, high frequency) and a = 1.1 nm (large amplitude, low frequency), for which the evaporation rates are identical. Snapshots of the latter case are shown in Figures 4(a−f). (The dynamics of the a = 0.1 nm case are qualitatively similar to the case in Figure 2, and are therefore not included here.) From Figure 4, when the droplet is vibrated at large amplitude with low frequency, significant oscillation of the contact line is observed. These oscillations can be seen in both the side and top views of the droplet, and resemble the "rocking mode" of vibration experimentally observed for macroscale drops.[36]

For these oscillating nanodroplets, the effects of amplitude and frequency on quantitative measures of interest (i.e., atomization and temperature) are shown in Figure 5. In Figure 5(a), the vibration amplitude is held constant at a = 0.5 nm and f is varied from 60−140 GHz, while in Figure 5(b), the vibration frequency is held constant at f = 200 GHz and a is varied from 0.1−0.4 nm (which is a range of subnanometre vibration amplitudes typical of SAW devices[13]). For the most part, the line-plots for the individual cases seem to follow expectations. With increasing f or a, an increase is observed both in the temperature within the droplet and the number of molecules atomized outside it. However, this trend is reversed for the cases with the largest a (with fixed f) and largest f (with fixed a). For example, for f = 140 GHz in Figure 5(a) and a = 0.4 nm in Figure 5(b) the droplet temperature appears to be lower when compared to the other cases, or mostly unchanged from the initial thermal condition of 300 K. The atomization

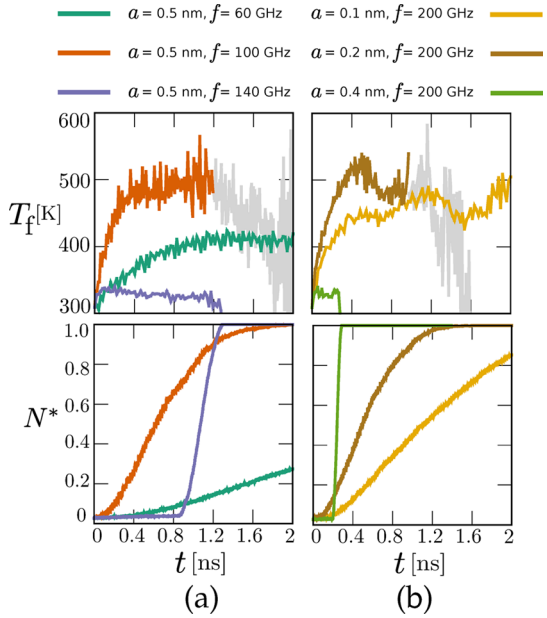

Figure 5. Temporal evolution of temperature (top row) and atomization (bottom row) for (a) multiple values of f for a fixed a = 0.5 nm, and (b) multiple values of a for a fixed f = 200 GHz; N_0 = 4500 and λ = 0.5 in all cases. The use of light gray indicates that our error threshold in the temperature measurements is exceeded.

DOI: 10.1021/acs.langmuir.8b02066
Langmuir 2018, 34, 11898−11904

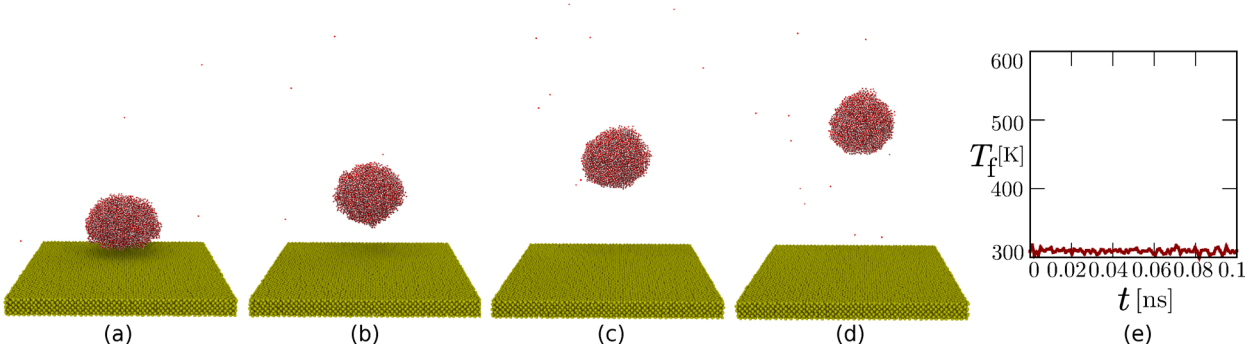

Figure 6. (a–d) MD snapshots and (e) time evolution of temperature, of a nanodroplet undergoing lift-off, at times t = 0.01, 0.05, 0.1, 0.15 ns, respectively. Case parameters: a = 0.5 nm, f = 100 GHz, N_0 = 4500, and λ = 0.15.

line-plots also show a sudden jump in N^* for both these cases, which is due to the whole droplet lifting beyond the 10 nm cutoff distance above the substrate. These two cases reveal a droplet lift-off phenomenon (as discussed in the next section); the behavior of oscillating droplets on a surface can indicate when droplet lift-off is imminent.

Nanodroplet Lift-Off. Figure 6 illustrates how a jump in the measured atomization, alongside a decrease in temperature, manifests physically: the substrate vibrations are strong enough to overcome the solid–liquid intermolecular forces and the droplet "lifts off" the surface (see Figure 6(b)). In the absence of gravitational forces, which are negligible at these scales, there is no restoring force preventing the droplet from continually rising until it collides with the superhydrophilic barrier at the top of the MD domain (Figure 6(c,d)). As a consequence of the breaking of the solid–fluid interaction, negligible heat is transferred to the droplet and its temperature is effectively unchanged from its original value of 300 K, as seen in Figure 6(e).

We systematically investigated the effect of vibration amplitude and frequency on this early droplet lift-off phenomenon, and the results are plotted as a phase map in Figure 7, with a resolution of 2 GHz and 0.1 nm. Open blue symbols represent cases where no lift-off is observed; solid teal symbols represent the *threshold* for lift-off; and solid purple symbols represent additional cases we simulated to confirm the lift-off threshold. The dotted line connecting the symbols divides the domain into "attached" and "lift-off" regions. The threshold frequency for lift-off is inversely dependent on the amplitude, monotonically decaying from ~180 GHz for a = 0.4 nm to 84 GHz when a = 1.0 nm. Note that, due to the computationally expensive nature of these MD simulations, this phase map was developed for the smallest nanodroplet used in our study, with N_0 = 1000. However, it is expected that any differences for larger nanodroplets would be limited to the (quantitative) threshold values for lift-off, while the qualitative variation in the stability threshold with amplitude would remain unchanged. Note that lift-off is more easily observed for low substrate wettabilities, i.e., low values of λ.

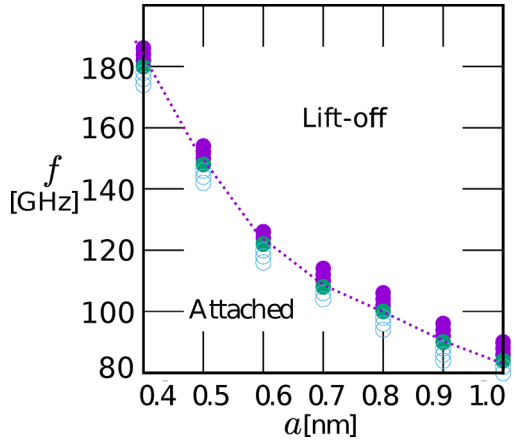

Figure 7. Phase map showing regions in the a–f landscape where nanodroplet lift-off is observed, for λ = 0.45 and N_0 = 1000. Note that the solid teal symbols represent the threshold for lift-off, while solid purple symbols represent cases where lift-off is observed, and open blue symbols are cases where it is not observed. A dotted line is drawn connecting the threshold cases to delineate the regions in this map.

Effect of substrate wettability. The role of surface wettability in vibration-induced atomization is investigated next. We conducted MD simulations for substrates with λ = 0.25, 0.5, 0.75, and 1.0. It is not straightforward to predict a priori how changing the wettability of the substrate will impact droplet atomization or lift-off. For example, it could be argued that the atomization process is controlled by the efficiency of energy transfer into the droplet, which is determined by the strength of the solid/liquid van der Waals forces. This would imply that the higher the wettability (λ), the stronger the interaction of the water molecules with the surface molecules (and so a larger contact area), and therefore a greater energy transfer and atomization rate. This argument has been shown to be correct in MD studies that focus solely on thermal energy transfer to a nanodroplet from a heated surface (with no vibrations): the higher the wettability, the higher the rate of the boiling/evaporation that can be achieved.[37]

Conversely, for any given water molecule, the energy barrier needing to be overcome for atomization would reduce with a weaker solid/liquid interaction. For low wettabilities (i.e., low λ), the liquid molecules require less energy to be dislodged from the solid and enter the vapor phase. This is consistent with observation of vibration-induced cavitation on patterned hydrophobic/hydrophilic surfaces: cavitation preferentially occurs on the hydrophobic sections,[38] indicating that vapor formation is quicker at lower wettabilities. This second argument would therefore imply that as wettability increases, the atomization rate should decrease.

As Figure 8(a) shows, both of these arguments are essentially correct, but they depend on the value of λ considered. As λ increases from 0.15 to 0.25, and from 0.25 to 0.50, the atomization rate increases, as is apparent when the values of N^* at any given time t are compared for λ = 0.15,

DOI: 10.1021/acs.langmuir.8b02066
Langmuir 2018, 34, 11898–11904

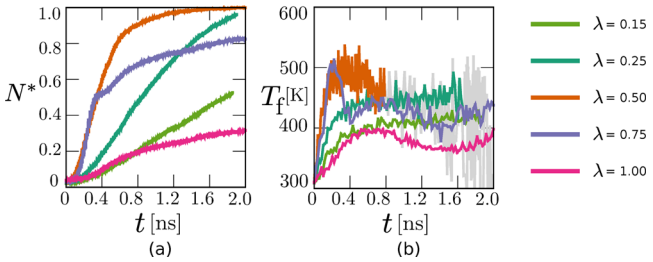

Figure 8. Time evolution of (a) the normalized atomization N^*, and (b) the droplet temperature T_f for a nanodroplet on surfaces of different wettabilities: λ = 0.15, 0.25, 0.50, 0.75, and 1.00. Other parameters are a = 0.375 nm, f = 100 GHz, and N_0 = 4500. The use of light gray indicates that our error threshold in the temperature measurements is exceeded.

0.25, or 0.50. Figure 8(b) shows that the relative increase in atomization rate can be traced to higher temperatures within the nanodroplets, indicating that the heat transfer between the vibrating substrate and the fluid is more efficient when the wettability is increased.

However, when λ increases from 0.50 to 0.75, and from 0.75 to 1.0, the atomization rate, rather than increasing, is observed to decrease. Figure 8(b) shows that this is only partly reflected in the temperature evolution. When comparing the temperature evolution of the λ = 0.50 and 0.75 cases, the temperature evolution and atomization are similar until $t \approx$ 0.3 ns, after which divergence is observed. This indicates that (a) the effect of increased energy transfer at higher wettabilities is outweighed by the larger number of stronger liquid/solid interactions that prevent droplet molecules from atomizing; and (b) a larger wetting area is more effective at conducting to the solid substrate the heat gained by the fluid, resulting in a decrease in droplet temperature for the λ = 0.75 case after t = 0.3 ns, relative to the λ = 0.50 case.

The temporal evolutions of atomization and droplet temperature for superhydrophobic and superhydrophilic surfaces, i.e., λ = 0.15 and 1.00, respectively, are strikingly similar (and lower throughout than the other surfaces). Due to physically distinct mechanisms, heat transfer into the droplet is inefficient in both cases, and neither surface is favored for atomization. The evaporation rate instead peaks when λ = 0.50, among the cases studied here, indicating that the optimal substrate for vibration-induced atomization is neither strongly hydrophobic nor strongly hydrophilic.

Note that this discussion has been limited to thermal evaporation, where the atomization occurs due to droplet heating. For low λ (or superhydrophobic) surfaces vibrating with large amplitudes, the droplets lift-off from the surface, rather than atomizing, as discussed previously.

CONCLUSIONS

We have used molecular dynamics (MD) simulations to study the dynamics of water nanodroplets on vertically vibrating metallic substrates. Our results have revealed numerous interesting vibration-induced phenomena at the nanoscale, including droplet evaporation, oscillation, and "lift-off". The effects of varying acoustic parameters (such as the amplitude and frequency of the substrate vibration), and physical parameters (such as the substrate wettability), have been investigated.

There are several new and fundamental insights. First, for nanodroplet evaporation, a universal scaling can be formulated, and the evaporation dynamics collapse onto a master curve for a fixed scaling parameter, A^*—the acoustothermal parameter. Second, nanodroplet oscillation is observed at large vibration amplitudes, likely due to high acoustic pressures being generated within the droplet. This produces a periodic rocking motion reminiscent of that seen in macroscale drops. Third, for larger vibration amplitudes or frequencies, the droplet is observed to take off from the surface entirely, particularly if the surface has a low wettability. A phase map has been developed to characterize this lift-off phenomenon, and shows that the threshold frequency of lift-off is inversely dependent on amplitude. Finally, evaporation is shown to be a slower process on a superhydrophobic or a superhydrophilic surface, and the optimal wettability for vibration-induced evaporation is neither too hydrophobic nor too hydrophilic.

The results presented in this paper can provide insight into the use of surface acoustics for numerous novel applications, for example:

- Acoustothermal droplet evaporation in evaporative self-assembly using nonvolatile solutes (nanotubes, nanowires, nanoparticles), as a simple route to creating highly ordered and complex structures.[28,29]
- Enhancing mixing within surface nanodroplets, with application to analytical chemistry.[39]
- A better understanding of how droplets can be shaken off surfaces is relevant to the development of acoustically enhanced self-cleaning[40] or ultrasonic drying.[32]
- The lift-off phenomenon could be a method for supplying cool droplets to hot spots in high heat-generating processor chips, circumventing the long timescales required for sessile droplets to coalesce and jump.[41,42]
- Tuning the evaporation characteristics via surface wettability is key to controlling energy dissipation in nanoscale devices,[43] or thermal management involving surface-driven phase change.[44]

This work can be developed in several directions. For example, the parametric study could be extended to include the effects of surface roughness and nanodroplet size on the phenomena observed; alternatively, mathematical models could be developed to predict the lift-off threshold or oscillation frequency as a function of the simulation parameters.

AUTHOR INFORMATION

Corresponding Author

*E-mail: r.pillai@ed.ac.uk.

ORCID

Matthew K. Borg: 0000-0002-7740-1932

Notes

The authors declare no competing financial interest.

ACKNOWLEDGMENTS

The authors thank the reviewers of this paper for their useful comments. The authors also thank the U.K.'s Engineering and Physical Sciences Research Council (EPSRC) for support under grant nos. EP/N016602/1 and EP/R007438/1, and the ARCHER UK National Supercomputing Service (http://www.archer.ac.uk). J.M.R. acknowledges the support of the Royal Academy of Engineering under the Chair in Emerging Technologies scheme. All data within this publication can be freely accessed at dx.doi.org/10.7488/ds/2432.

DOI: 10.1021/acs.langmuir.8b02066
Langmuir 2018, 34, 11898−11904

REFERENCES

(1) Rayleigh, L. On the capillary phenomena of jets. *Proc. R. Soc. London* **1879**, *29*, 71−97.
(2) Lamb, H. *Hydrodynamics*; Cambridge University Press: Cambridge/New York, 1932; p 475.
(3) Landau, L. D.; Lifshitz, L. L. *Fluid Mechanics*; Pergamon: New York, 1984; p 244.
(4) Nyborg, W. L. Acoustic Streaming due to Attenuated Plane Waves. *J. Acoust. Soc. Am.* **1953**, *25*, 68.
(5) Lighthill, S. J. Acoustic streaming. *Journal of Sound and Vibration* **1978**, *61*, 391−418.
(6) Vukasinovic, B.; Glezer, A.; Smith, M. K. Vibration-Induced Droplet Atomization. *Phys. Fluids* **2000**, *12*, S12.
(7) Vukasinovic, B.; Smith, M. K.; Glezer, A. Spray characterization during vibration-induced drop atomization. *Phys. Fluids* **2004**, *16*, 306−316.
(8) Vukasinovic, B.; Smith, M. K.; Glezer, A. Mechanisms of free-surface breakup in vibration-induced liquid atomization. *Phys. Fluids* **2007**, *19*, 012104.
(9) Jimmy, B.; Kolev, S. D.; Kentish, S.; Ashokkumar, M. A novel approach for enhancing metal ion separation using acoustic nebulisation. *Ultrason. Sonochem.* **2012**, *19*, 435−439.
(10) Momen, A. M.; Kokou, E.; Bansal, P.; Gluesenkamp, K. R.; Abdelaziz, O. Preliminary investigation of novel direct contact ultrasonic clothes drying process. *Proceedings of the ASME 2015 International Mechanical Engineering Congress & and Exposition* **2015**, 1−7.
(11) Monkkonen, L.; Edgar, J. S.; Winters, D.; Heron, S. R.; Mackay, C. L.; Masselon, C. D.; Stokes, A. A.; Langridge-Smith, P. R. R.; Goodlett, D. R. Screen-printed digital microfluidics combined with surface acoustic wave nebulization for hydrogen-deuterium exchange measurements. *Journal of Chromatography A* **2016**, *1439*, 161−166.
(12) Friend, J.; Yeo, L. Y. Microscale acoustofluidics: Microfluidics driven via acoustics and ultrasonics. *Rev. Mod. Phys.* **2011**, *83*, 647−704.
(13) Yeo, L. Y.; Friend, J. R. Surface Acoustic Wave Microfluidics. *Annu. Rev. Fluid Mech.* **2014**, *46*, 379−406.
(14) Choi, J. D.; Feurer, T.; Yamaguchi, M.; Paxton, B.; Nelson, K. A. Generation of ultrahigh-frequency tunable acoustic waves. *Appl. Phys. Lett.* **2005**, *87*, 081907.
(15) Ivry, Y.; Wang, N.; Durkan, C. High-frequency programmable acoustic wave device realized through ferroelectric domain engineering. *Appl. Phys. Lett.* **2014**, *104*, 133505.
(16) Shilton, R. J.; Travagliati, M.; Beltram, F.; Cecchini, M. Nanoliter-droplet acoustic streaming via ultra high frequency surface acoustic waves. *Adv. Mater.* **2014**, *26*, 4941−4946.
(17) Matsuda, O.; Wright, O. B. *Frontiers in Optical Methods*; Springer, 2014; pp 129−151.
(18) Dong, L.; Chaudhury, A.; Chaudhury, M. K. Lateral vibration of a water drop and its motion on a vibrating surface. *Eur. Phys. J. E: Soft Matter Biol. Phys.* **2006**, *21*, 231−242.
(19) Alghane, M.; Chen, B. X.; Fu, Y. Q.; Li, Y.; Luo, J. K.; Walton, a. J. Experimental and numerical investigation of acoustic streaming excited by using a surface acoustic wave device on a 128° YX-LiNbO3 substrate. *J. Micromech. Microeng.* **2011**, *21*, 015005.
(20) Alghane, M.; Fu, Y. Q.; Chen, B. X.; Li, Y.; Desmulliez, M. P. Y.; Walton, A. J. Streaming phenomena in microdroplets induced by Rayleigh surface acoustic wave. *J. Appl. Phys.* **2011**, *109*, 114901.
(21) Alghane, M.; Fu, Y. Q.; Chen, B. X.; Li, Y.; Desmulliez, M. P. Y.; Walton, A. J. Frequency effect on streaming phenomenon induced by Rayleigh surface acoustic wave in microdroplets. *J. Appl. Phys.* **2012**, *112*, 084902.
(22) Alghane, M.; Fu, Y. Q.; Chen, B. X.; Li, Y.; Desmulliez, M. P. Y.; Walton, A. J. Scaling effects on flow hydrodynamics of confined microdroplets induced by Rayleigh surface acoustic wave. *Microfluid. Nanofluid.* **2012**, *13*, 919−927.
(23) Alghane, M.; Chen, B. X.; Fu, Y. Q.; Li, Y.; Desmulliez, M. P. Y.; Mohammed, M. I.; Walton, A. J. Nonlinear hydrodynamic effects induced by Rayleigh surface acoustic wave in sessile droplets. *Physical Review E - Statistical, Nonlinear, and Soft Matter Physics* **2012**, *86*, 2−7.
(24) Riaud, A.; Baudoin, M.; Bou Matar, O.; Thomas, J.-L.; Brunet, P. On the influence of viscosity and caustics on acoustic streaming in sessile droplets: an experimental and a numerical study with a cost-effective method. *J. Fluid Mech.* **2017**, *821*, 384−420.
(25) Abascal, J. L.; Vega, C. A general purpose model for the condensed phases of water: TIP4P/2005. *J. Chem. Phys.* **2005**, *123*, 234505.
(26) Ryckaert, J. P.; Ciccotti, G.; Berendsen, H. J. Numerical integration of the cartesian equations of motion of a system with constraints: molecular dynamics of n-alkanes. *J. Comput. Phys.* **1977**, *23*, 327−341.
(27) Plimpton, S. Fast parallel algorithms for short-range molecular dynamics. *J. Comput. Phys.* **1995**, *117*, 1−19.
(28) Zhang, J.; Borg, M. K.; Sefiane, K.; Reese, J. M. Wetting and evaporation of salt-water nanodroplets: A molecular dynamics investigation. *Phys. Rev. E* **2015**, *92*, 1−11.
(29) Zhang, J.; Borg, M. K.; Ritos, K.; Reese, J. M. Electrowetting Controls the Deposit Patterns of Evaporated Salt Water Nanodroplets. *Langmuir* **2016**, *32*, 1542−1549.
(30) Avvaru, B.; Patil, M. N.; Gogate, P. R.; Pandit, A. B. Ultrasonic atomization: Effect of liquid phase properties. *Ultrasonics* **2006**, *44*, 146−158.
(31) Kentish, S.; Ashokkumar, M. *Ultrasound Technologies for Food and Bioprocessing* **2011**, 1−12.
(32) Peng, C.; Ravi, S.; Patel, V. K.; Momen, A. M.; Moghaddam, S. Physics of direct-contact ultrasonic cloth drying process. *Energy* **2017**, *125*, 498−508.
(33) Hadjiconstantinou, N. G.; Garcia, A. L.; Bazant, M. Z.; He, G. Statistical error in particle simulations of hydrodynamic phenomena. *J. Comput. Phys.* **2003**, *187*, 274−297.
(34) Pillai, R.; Borg, M. K.; Reese, J. M. Acoustothermal atomization of water nanofilms. *Phys. Rev. Lett.* **2018**, *121*, 104502.
(35) Galleguillos-Silva, R.; Vargas-Hernández, Y.; Gaete-Garretón, L. Wettability of a surface subjected to high frequency mechanical vibrations. *Ultrason. Sonochem.* **2017**, *35*, 134−141.
(36) Milne, A. J. B.; Defez, B.; Cabrerizo-Vílchez, M.; Amirfazli, A. Understanding (sessile/constrained) bubble and drop oscillations. *Adv. Colloid Interface Sci.* **2014**, *203*, 22−36.
(37) Hens, A.; Agarwal, R.; Biswas, G. Nanoscale study of boiling and evaporation in a liquid Ar film on a Pt heater using molecular dynamics simulation. *Int. J. Heat Mass Transfer* **2014**, *71*, 303−312.
(38) Belova-Magri, V.; Brotchie, A.; Cairós, C.; Mettin, R.; Möhwald, H. Micropatterning for the control of surface cavitation: Visualization through high-speed imaging. *ACS Appl. Mater. Interfaces* **2015**, *7*, 4100−4108.
(39) Yu, H.; Peng, S.; Lei, L.; Zhang, J.; Greaves, T. L.; Zhang, X. Large Scale Flow-Mediated Formation and Potential Applications of Surface Nanodroplets. *ACS Appl. Mater. Interfaces* **2016**, *8*, 22679−22687.
(40) Ragesh, P.; Anand Ganesh, V.; Nair, S. V.; Nair, A. S. A review on 'self-cleaning and multifunctional materials'. *J. Mater. Chem. A* **2014**, *2*, 14773−14797.
(41) Enright, R.; Miljkovic, N.; Sprittles, J.; Nolan, K.; Mitchell, R.; Wang, E. N. How coalescing droplets jump. *ACS Nano* **2014**, *8*, 10352−10362.
(42) Cha, H.; Xu, C.; Sotelo, J.; Chun, J. M.; Yokoyama, Y.; Enright, R.; Miljkovic, N. Coalescence-induced nanodroplet jumping. *Physical Review Fluids* **2016**, *1*, 064102.
(43) Pop, E. Energy dissipation and transport in nanoscale devices. *Nano Res.* **2010**, *3*, 147−169.
(44) Attinger, D.; Frankiewicz, C.; Betz, A. R.; Schutzius, T. M.; Ganguly, R.; Das, A.; Kim, C.-J.; Megaridis, C. M. Surface engineering for phase change heat transfer: A review. *MRS Energy & Sustainability* **2014**, *1*, E4.

DOI: 10.1021/acs.langmuir.8b02066
Langmuir 2018, 34, 11898−11904